Si WENRONG, Fu CHENZHAO, Gao KAI, Huang HUA, Ni HAO

East China Electric Power Test & Research Institute Company Limited, Shanghai, China

Study on time-frequency extractors for partial discharge pulse current used in sequence grouping and identification

Abstract*. This paper introduces a general way to make feature extraction for partial discharge (PD) pulse waveshape used in sequence grouping resorting with equivalent time-frequency method. A digital ac PD pulse detection system with bandwidth of 10 kHz - 40 MHz and sampling rate of 100 MS/s is introduced, which was developed to study those feature extractors. Simulation and test results with gas insulated switch (GIS) show that they are practical and effective to develop PD detection system with grouping and identification technique.*

Streszczenie. *Dokonano ekstrakcji impulsu wyładowania niezupełnego przy wykorzystaniu odpowiedniej metody czasowo-częstotliwościowej. Wykorzystano system cyfrowy z pasmem 10 kHz – 40 MHz i częstotliwością próbkowania 100 MS/s. Badania wyłącznika gazowego potwierdziły skuteczność metody. (**Czasowo-częstotliwościowa ekstrakcja i identyfikacja impulsu wyładowania niezupełnego**)*

Keywords: partial discharge; pulse current; feature extraction; grouping; identification.
Słowa kluczowe: wyładowanie niezupełne, impuls prądowy, identyfiakcja.

Introduction

PD detection has almost become the most popular method to evaluate dielectric insulation condition at ac voltage applications [1-5]. For this, there are different kinds of PD measurement systems developed based on pulse current detection (the standard method) [6], UHF detection [7], acoustic detection [8] and even optical detection [9], with advantages and disadvantages respectively. Most of those conventional PD detection systems make the analysis of PD data, with assuming implicitly the presence of only one PD phenomenon (Fig. 1). But in operation conditions, more than one pulse source may be active due to the presence of either a plurality of defects or electrical noise, sometimes even both [10-12]. Different PD phenomena simultaneously active can combine in a mixed PD pulse sequence. To this problem, conventional PD detection systems suffer a major drawback. They only collect incoming pulse signals and compress the information in two parameters: the arrival time (phase) and the magnitude. In order to avoid noise and external interference pulses to be detected, these detection systems allow the operator to select different input filters. However, even in the ideal case of complete noise suppression, they may provide PD patterns that can be made of the superposition of different PD and noise sources. Thus, the different PD phenomena simultaneously active can be mixed in the different histograms deduced from the analysis of pulse height and phase distributions, which is currently used for diagnosis purpose. So those devices could fail to deal with the multi-PD sources.

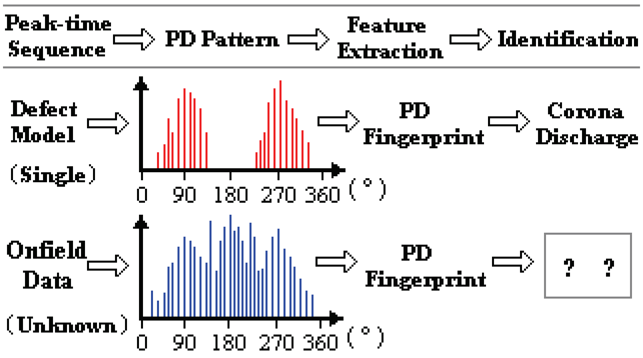

Fig.1. Flowcharts of the conventional ac PD measurement system (peak-detection instruments)

Presently, a novel measurement system for ac PD that uses a pulse sequence grouping technique (Fig. 2) before the PD identification was presented in references [10-12]. It fully exploits the information carried by the PD pulse waveshape. On-board electronics and artificial intelligence tools enable to sort out sub-groups of pulse sequence, each of them relevant to one PD signal or noise source. Then some post-processing is applied to those sub-groups of different pulse signals, including noise rejection, identification and diagnosis. A simple dc PD pulse wideband detection system was developed with pulse source separation technique [13], which is also capable of handing noise suppression and multi-PD sources classification at dc voltage. Besides the grouping technique developed resorting to current pulse with wideband detection, reference [14] introduced remote radiometric measurements for detecting PD behavior in power transformer. All of those works [10-14] give a result that the pulse sequence grouping is useful for the PD measurement system, which is capable of handling noise rejection and multi-PD sources.

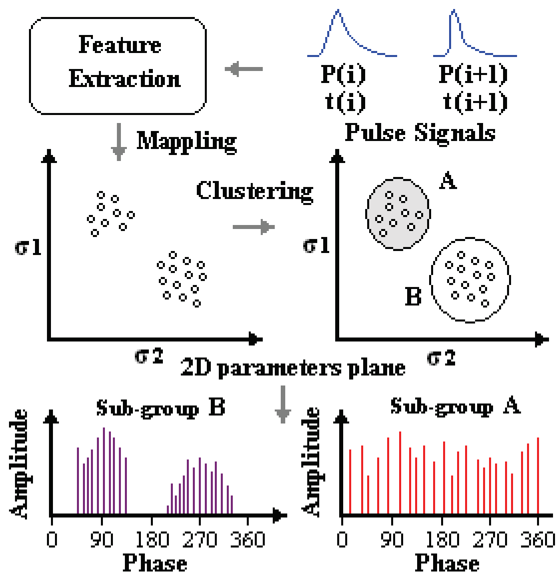

Fig.2. Architecture of PD pulse sequence grouping

In design of a PD measurement system with pulse sequence grouping technique, finding a set of features corresponding to an optimal grouping performance (accuracy and reliability) is critical. A PD diagnostic system designer typically does not have much difficulty to obtain a large number of features by applying different feature extraction methods on PD pulse waveshapes. However, the designer often faces challenges in finding a set of features which may give the optimal grouping performance. The primary reasons for that may be [15]: a) features cannot be evaluated individually since feature interaction may affect the grouping performance more significantly than features themselves; b) optimal features cannot be obtained by simply combining all features from different feature extraction methods since there exist redundant and irrelevant features; and c) a separability criterion should be applied to the feature extraction methods for analyzing their performance on the grouping objects before integrated into the measurement system.

This paper attempts to address the challenge by the following content. Firstly, according to the PD wideband detection system with sequence grouping technique, based on those pioneered works [10-15], and some works related to PD pulse waveshape, a general way to make feature extraction for PD pulse waveshape used in sequence grouping is given. As an example, three feature extractors are obtained with post-processing methods applied to PD pulse waveshape in time and frequency domains, which are equivalent evaluation, autocorrelation and information measure. And a separability criterion for pulse feature extractors is defined and analyzed with PD pulse sequences generated by the combination of exponential models and Monte Carlo simulation. Then, a digital ac PD pulse detection system with bandwidth of 10 kHz – 40 MHz and sampling rate of 100 MS/s is introduced, which was developed to study of those feature extractors used in PD pulse grouping. At last, Experimental verification is made resorting to the PD pulse detection system for GIS artificial models tests and simulation test of two PD calibrators, which makes an investigation on the grouping performance of the feature extractors for an online field PD pulse signals.

PD pulse feature extraction

Actually, PD pulse feature extraction is a mapping tool, which provides a compact and meaningful representation of the measured pulses embedded in the waveshapes in time domain and allows fast post-processing. In other words, the samples relevant to a single pulse waveshape should be compressed into a few numbers (two or three parameters), each of them bringing essential information. In Fig. 3, a general way to make feature extraction for PD pulse is shown. PD pulses are characterized by points in 2D Cartesian parameters plane (σ_1,σ_2) or 3D Cartesian parameters space $(\sigma_1,\sigma_2,\sigma_3)$ [13], then visual inspection of results can be achieved with image representation. The parameters σ_1, σ_2 and σ_3 may or not have relationship of each other. The values of them are decided by the transform (T) and functions (F) in Fig. 3 chosen by the PD detection system designer. A lot of feature extraction methods are available, if different transforms and linear or nonlinear functions are used. But an efficient mapping tool for PD pulse waveshapes at least should be amplitude, polarity and shift independent [10]. And the most important is that the formed parameters should be with good separability to stochastic pulse waveshapes of different PD sources or pulsed interference signals, with consideration of a good compromise between complexity of computations and real-time requirements. In this paper, FFT is chosen as the transform applied to PD pulse in time domain, so all the feature extractors obtained are based on PD pulse waveshapes in time and frequency domains with different functions respectively, which will be shown in the following.

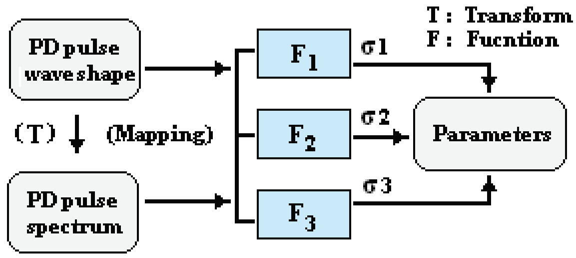

Fig.3. A general way of feature extraction for PD pulse waveshape

A simple way to characterize a signal $p(t)$ simultaneously in time and frequency is to consider its mean localizations and dispersions. This can be obtained by considering $|p(t)|^2$ and $|P(f)|^2$ as probability distributions, and looking at their mean values and standard deviations [16]:

$$(1)\qquad \begin{cases} t_0 = (1/E_p)\int_{-\infty}^{+\infty} t\,|p(t)|^2\,dt \\ f_0 = (1/E_p)\int_{-\infty}^{+\infty} f\,|P(f)|^2\,df \\ T^2 = (4\pi/E_p)\int_{-\infty}^{+\infty} (t-t_0)^2\,|p(t)|^2\,dt \\ F^2 = (4\pi/E_p)\int_{-\infty}^{+\infty} (f-f_0)^2\,|P(f)|^2\,df \end{cases}$$

where: $E_p = \int_{-\infty}^{+\infty} |p(t)|^2\,dt$.

Then a signal can be characterized in the time-frequency plane by its mean position (t_0, f_0) and a domain of main energy localization whose area is proportional to $T\times F$.

According to Fig. 3, the (T,F) and (T,F,TF) named equivalent time-frequency method (ETFM) are chosen to be the feature extractors for PD pulse signals, where $TF = T\times F$. The (T,F) plane is called "equivalent time-length and bandwidth" plane in reference [10-13], has already been verified that it can be successfully employed for achieving noise rejection and sources separation of ac PD and dc PD.

Autocorrelation is a special digital signal processing method [17] that has the ability to extract a measurement signal when it is completely swamped by noise, i.e. when the noise amplitude is larger than the signal amplitude. Unfortunately, phase information in the measurement signal is lost during the autocorrelation process, but the amplitude and frequency can be extracted accurately. For a measurement signal $p(t)$, the autocorrelation coefficient R_p is the average value of the product of $p(t)$ and $p(t-\tau)$, where $p(t-\tau)$ is the value of the measurement signal delayed by a time τ. The autocorrelation function $R_p(\tau)$ describes the relationship between R_p and τ as τ varies:

$$(2)\qquad R_p(\tau) = \lim_{\tau\to\infty}\left[\int_{-T}^{T} p(t)p(t-\tau)dt/(2T)\right]$$

For the PD pulse signal $p(t_k), k = 0,1,2,\cdots n-1$ sampled by the detection system with k points, its function $R_p(m)$ can be defined as: $R_p(m) = \sum_{k=0}^{n-1} p(t_k)p(t_{k+m})/n$. Apparently, $R_p(m)$ can be chosen as the parameters to make representation of the measured pulses. Based on this, a representation of the measured pulses named time-frequency autocorrelation method (TFACM) is described as:

(3)
$$\begin{cases} R_t(0) = \frac{1}{n}\sum_{k=0}^{n-1} p(t_k)p(t_k) \\ R_f(0) = \frac{2}{n}\sum_{k=0}^{n/2-1} P(f_k)P(f_k) \\ R_t(m) = \frac{1}{n}\sum_{k=0}^{n-1} p(t_k)p(t_{k+m})/R_t(0) \\ R_f(m) = \frac{2}{n}\sum_{k=0}^{n/2-1} P(f_k)P(f_{k+m})/R_f(0) \end{cases}$$

where: $R_t(0)$ and $R_f(0)$ – the maximum value of autocorrelation coefficients of $p(t)$ in time domain and $P(f)$ in frequency domain, respectively.

Then a PD pulse signal can be characterized in the time-frequency autocorrelation plane by $(R_t(m), R_f(m))$. The $(R_t(m), R_f(m), R_{tf}(m))$ is also chosen to be the feature extractors for PD pulse signals according to Fig. 3, where $R_{tf}(m) = R_t(m)\times R_f(m)$.

Is there a simple definition which can describe the pulse signal for its special characteristic? A solution is given by applying an information measure to the signal $p(t)$. This information, known as Renyi information [17], is given by

(4) $$Ri_t^n = \log_2[\int_{-\infty}^{+\infty} p^n(t)dt]/(n-1)$$

where: the result by this measure is expressed in bits.

So here comes another compact and meaningful representation of the measured PD pulses named time-frequency entropy method (TFEM) described as:

(5)
$$\begin{cases} Ri_t^2 = -\log_2[\sum_{k=0}^{n-1}(t_k - t_0)^2 \cdot p^2(t_k)/\sum_{k=0}^{n-1} p^2(t_k)] \\ Ri_f^2 = -\log_2[\sum_{k=0}^{n/2}(f_k - f_0)^2 \cdot P^2(f_k)/\sum_{k=0}^{n/2} P^2(f_k)] \end{cases}$$

where: Ri_t^2 and Ri_f^2 – the second order Renyi information of $p(t)$ in time domain and $P(f)$ in frequency domain.

Then a PD pulse signal can be characterized in the time-frequency entropy plane by (Ri_t^2, Ri_f^2) and space by $(Ri_t^2, Ri_f^2, Ri_{tf}^2)$, where $Ri_{tf}^2 = Ri_t^2 \times Ri_f^2$.

Separability criterion for PD pulse feature extractions

In this section, a separability criterion for PD pulse feature extractors is defined. Before its application to the feature extraction results of the parameter extractors introduced in section 2 for an online field PD pulse signals, the ones of simulation PD pulse sequence are analyzed to show the grouping performance, theoretically. So in the following, simulation PD pulse sequence used in this section will be given before the definition of separability criterion.

Past investigations carried out to analyze PD signals were shown that different PD sources generated current pulses with a considerable variety of shapes [3, 10, 15-17]. And the PD signals detected at the terminals of tested object are the convolution of the signal generated by PD source with the dynamic impedance of transmission path, which makes their shapes distorted in an unpredictable way. But most of the detected PD pulse signal can be described approximately with different exponential models (EMs) in the following [18, 19]:

(6)
$$\begin{cases} P_1(x) = Ae^{-t/\tau} \\ P_2(x) = Ae^{-t/\tau}\sin 2\pi f_c t \\ P_3(x) = A(e^{-t/\tau_1} - e^{-t/\tau_2}) \\ P_4(x) = A(e^{-t/\tau_1} - e^{-t/\tau_2})\sin 2\pi f_c t \end{cases}$$

where: A – the amplitude, τ –the attenuation rate and f_c – the oscillation frequency of the PD pulse signal, respectively.

In Fig. 4, noised simulation PD pulse signals generated using the expression (6) is shown.

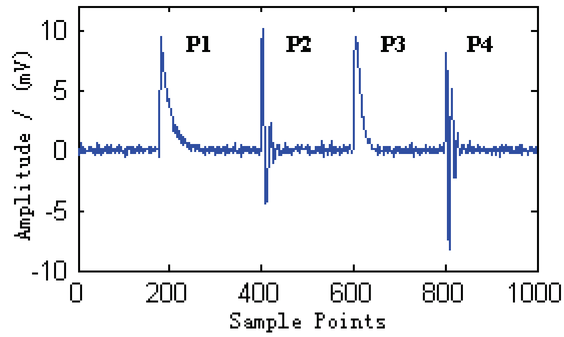

Fig.4. Simulation PD pulse signals generated with EMs

Four PD pulse sequences generated by combination of EMs and Monte Carlo simulation (MCS) are shown in Fig. 5, where each one is corresponding to the pulse in Fig. 4. MCS is a method for iteratively evaluating a deterministic mode using sets of random numbers as inputs. It was once used in reference [20] to simulate the PD distribution of GIGRE Method II electrode system. Here, the way of MCS with combination of the EMs to generate PD pulse sequence is defined as five steps:

1): Choose a parametric model, such as $P_2(x)$ in (6).

2): Generate a set of random inputs ξ_1, ξ_2 and ξ_3 with a certain distribution, such as hypodispersion. Redefine the parametric model:

(7) $$P_2(x) = (A+\xi_1)e^{-t/(\tau+\xi_2)}\sin 2\pi(f_c + \xi_3)t$$

3): Evaluate the model and store the results as $P_2^i(x)$.

4): Repeat steps 2 and 3 for $i = 1,\cdots,n$.

5): Make feature extraction for $P_2^i(x), i = 1,\cdots,n$.

where in 5), feature extraction is made to the simulation results (PD pulse sequence) instead of conventional analysis such as histogram, summary statistics and confidence intervals, etc. The feature extraction results with application of ETFM, TFACM and TFEM are shown in the Fig. 6, which will be evaluated by the separation criterion defined in following content.

For the set $\{\sigma_i\}_A, i = 1,2,\cdots,k$ ($\{\sigma_i\}_A = (\sigma_{1i}^A, \sigma_{2i}^A)$ for 2D feature extraction and $\{\sigma_i\}_A = (\sigma_{1i}^A, \sigma_{2i}^A, \sigma_{3i}^A)$ for 3D feature extraction) formed by the same feature extractor to the pulse sequence A, the distance between $\{\sigma_i\}_A, i = 1,2,\cdots,k$ can be treated as one of the most important measures to analyze the performance. The mean value of the distance between all elements in set $\{\sigma_i\}_A, i = 1,2,\cdots,k$ can be defined as

(8) $$D_{i,j}^2(\{\sigma_i\}_A, \{\sigma_j\}_A) = \sum_{i=1}^{k}\sum_{j=1}^{k} D^2(\sigma_i^A, \sigma_j^A)/(k\cdot(k-1))$$

where: $D^2(\sigma_i^A, \sigma_j^A)$ – the distance between element $\{\sigma_i\}_A$ and $\{\sigma_j\}_A$.

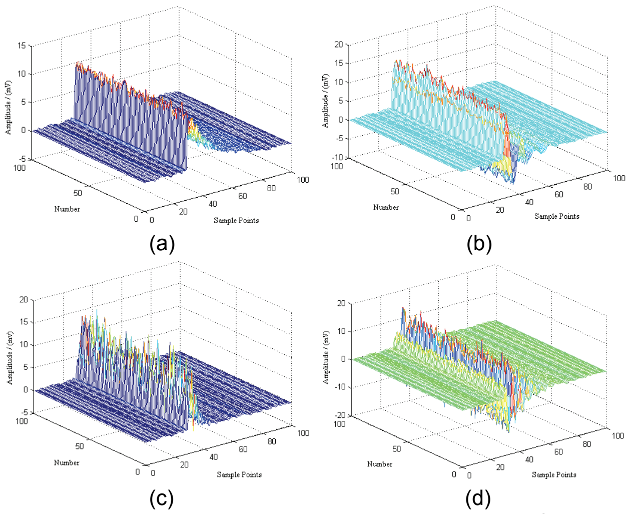

Fig.5. PD pulse sequences generated by combination of EMs and MCS: (a) is sequence A with pulse waveshape P1 in Fig. 4; (b) is sequence B with pulse waveshape P2 in Fig. 4; (c) is sequence C with pulse waveshape P3 in Fig. 4; (d) is sequence D with pulse waveshape P4 in Fig. 4

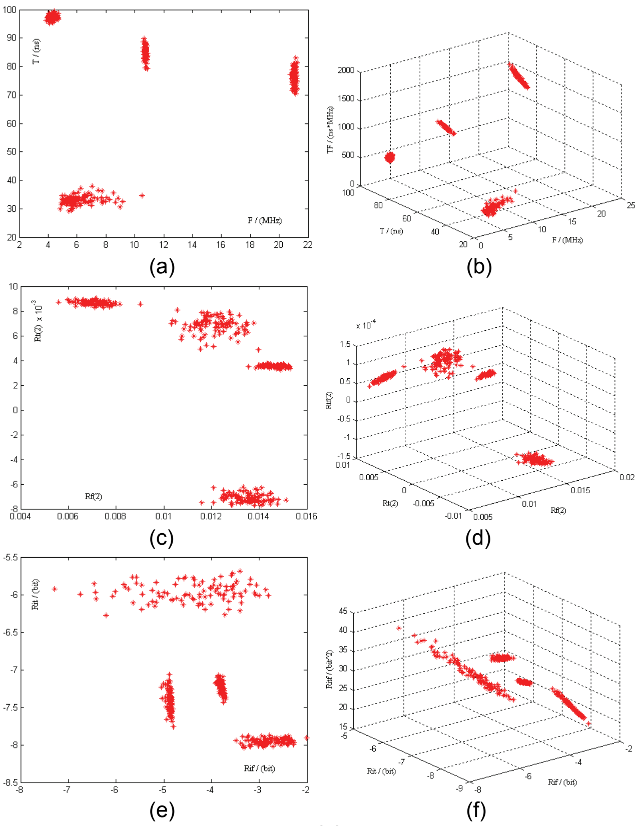

Fig.6. Results with application of feature extractors introduced in section 2 to the PD pulse sequences of Fig. 5: (a) and (b) are 2D and 3D feature extraction results using ETFM; (c) and (d) are 2D and 3D feature extraction results using TFACM; (e) and (f) are 2D and 3D feature extraction results using TFEM

The distance $D^2(\sigma_i,\sigma_j)_A$ can be defined as the 3D feature extractor applied to PD pulse waveshape:

(9) $$D^2(\sigma_i,\sigma_j)_A=(\sigma_{1i}^A-\sigma_{1j}^A)^2+(\sigma_{2i}^A-\sigma_{2j}^A)^2+(\sigma_{3i}^A-\sigma_{3j}^A)^2$$

For the set $\{\sigma_i\}_A, i=1,2,\cdots,k_A$ and set $\{\sigma_i\}_B, i=1,\ 2,\cdots,k_B$ formed by the same feature extractor applied to two different pulse sequences A and B, the mean value of the distance between all elements in sets $\{\sigma_i\}_A, i=1,2,\cdots,k_A$ and $\{\sigma_i\}_B, i=1,2,\cdots,k_B$ can be defined as

(10) $$D_{i,j}^2(\{\sigma_i\}_A,\{\sigma_j\}_B)=\sum_{i=1}^{k_A}\sum_{j=1}^{k_B}D^2(\sigma_i^A,\sigma_j^B)/(k_A\cdot k_B)$$

where: $D^2(\sigma_i^A,\sigma_j^B)$ – the distance between element $\{\sigma_i\}_A$ and $\{\sigma_j\}_B$.

It has the same definition as the expression (9). Apparently, if the $D_{i,j}^2(\{\sigma_i\}_A,\{\sigma_j\}_A)$ or $D_{i,j}^2(\{\sigma_i\}_B,\{\sigma_j\}_B)$ are with small values and $D_{i,j}^2(\{\sigma_i\}_A,\{\sigma_j\}_B)$ is with big value, the feature extractor applied to PD pulse sequence A and B is effective. So with the expressions (9) and (10), the separability criterion to evaluate the performance of feature extraction methods for PD pulse sequence grouping can be defined as

(11) $$J_{A,B}^{D^2}=\frac{D_{i,j}^2(\{\sigma_i\}_A,\{\sigma_j\}_B)}{D_{i,j}^2(\{\sigma_i\}_A,\{\sigma_j\}_A)+D_{i,j}^2(\{\sigma_i\}_B,\{\sigma_j\}_B)}$$

where: $J_{A,B}^{D^2}>1$ means that the feature extractor applied to pulse sequences A and B for grouping has good property, while $J_{A,B}^{D^2}\le 1$ means poor property.

Table 1 to 3 shows the corresponding values of separability measure with (2D, 3D) form, which are obtained by application of expressions (8), (9) and (11) to the feature extraction results shown in Fig. 6. The mean values of separability measure using ETFM, TFACM and TFEM are (5.59, 8.94), (5.58, 6.52) and (2.15, 2.40), which gives a result that all feature extractor have good performance used in PD pulse sequence grouping.

Table 1. Values of separability measure of ETFM (2D, 3D)

	A	B	C	D
A	1.18, 29.1		$D_{i,j}^2$	
B	14.5, 493	2.81, 29.6		
C	64.6, 226	52.0, 707	2.66, 56.3	
D	27.2,1194	48.0, 1573	46.0, 1407	3.98, 84.3
A	0, 0		$J_{A,B}^{D^2}$	
B	3.64, 8.41	0, 0		
C	1.12, 2.65	9.51, 8.24	0,0	
D	5.27, 10.5	7.07, 13.8	6.92, 10.0	0, 0

Table 2. Values of separability measure of ETFM (2D, 3D)

	A	B	C	D
A	7.5, 7.9		$D_{i,j}^2$	
B	91.8, 122	5.42, 6.42		
C	55.5 80.2	42.9, 64.4	14.7, 18.7	
D	171,211	108, 137	142, 201	10.6, 11.6
A	0, 0		$J_{A,B}^{D^2}$	
B	7.09, 8.50	0, 0		
C	2.49, 3.01	2.13, 2.56	0, 0	
D	9.45, 10.8	6.74, 7.61	5.59, 6.64	0, 0

Table 3. Values of separability measure of ETFM (2D, 3D)

	A	B	C	D
A	0.44, 3.55		$D_{i,j}^2$	
B	1.29, 6.07	0.13, 0.36		
C	2.78, 8.12	1.72, 6.21	1.38, 8.39	
D	2.20,14.49	1.11, 8.81	1.82, 11.6	0.20, 0.91
A	0, 0		$J_{A,B}^{D^2}$	
B	2.26, 1.55	0, 0		
C	1.53, 0.68	1.14, 0.71	0, 0	
D	3.43, 3.25	3.36, 6.94	1.15, 1.25	0, 0

A lot of values of separability measure were obtained resorting to feature extraction results from different simulation PD pulse sequences, which shows almost the same analysis result shown in the above. This gives a theoretical approve that those feature extractors (ETFM, TFACM and TFEM) are capable of process the PD pulse.

AC PD measuring system description

For many applications, it has been observed that a bandwidth up to 40 MHz, associated with a digitizer as fast as 100 MS/s is sufficient to provide enough information for PD signals detection [10, 13]. In Fig. 7, a simple measuring system for the digital acquisition of ac PD current pulse signals was being developed resorting to a fast digitizer of NI5112 type (its analog bandwidth is 100 MHz, the maximum sample rate is 100 MS/s and the memory length is 16 MS in each channel). A 10 kHz to 40 MHz hardware bandwidth limit is imposed to remove unwanted low-frequency and high-frequency noise for the signal detection Channel A. Channel A is connected to the measuring impedance in the test circuit, while Channel B is connected to a voltage divider allows the synchronization of PD signals acquisition with the applied voltage.

In Fig. 7, the trigger source, trigger type, trigger level, trigger slope, min sample rate and min sample length of the digitizer are set to be Channel B, trigger Edge, 0, Positive, 100 MS/s and 2 MS, respectively. These parameters mean that the detection system only works when Channel B gets a coming AC voltage signal at its zero phase, then after Channel A samples signals from detection impedance with 2MS (100 MS/s×20 ms = 2 MS), the system stops and will work again until the coming AC voltage signal at its another zero phase. For the frequency of AC voltage is 50 Hz in China, so 20 ms is one period of AC voltage.

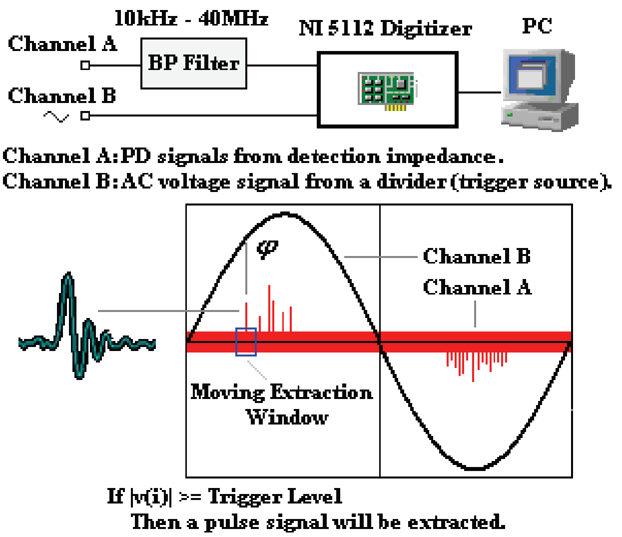

Fig.7. Description of the developed ac PD measuring system

The next work is to extract PD pulse waveshapes and their corresponding phase information within the 2 MS sampled by Channel A, using a moving extraction window (MEW) shown in Fig. 7. The phase value is easy to get for the i[th] point within 2 MS: phase(i)=360*i/2M (φ in Fig. 7). The PD pulse signals can be extracted using MEW with a threshold value and a simple algorithm. The length of MEW *k* can be 100 (1 us), 200 (2 us), 300 (3 us), ……, 1000 (10 us) points to fit for PD pulse waveshape and other pulsed interference signals. With this method, lots of pulses will be obtained after processing periods up to 200 if a PD source exists.

For considering the practical application to the PD pulse sequence in the flied monitoring system, the preprocessing for a single pulse waveshape $p_j(t)$ and its FFT spectrum $P_j(f)$ recorded with *k* points should be done is defined as:

(12) $$p_j(t)=\begin{cases} p_0, p_1, \cdots, p_i, \cdots, p_{k-1} \\ 0, \Delta t, \cdots, \Delta t(i-1), \cdots \Delta t(k-1) \end{cases}$$

(13) $$P_j(f)=\begin{cases} P_0, P_1, \cdots, P_i, \cdots, P_{k/2-1} \\ 0, \Delta f, \cdots, \Delta f(i-1), \cdots \Delta f(k/2-1) \end{cases}$$

for $j=1,2,\cdots,N$ (N is the total number of pulse waveshapes) and $i=1,2,\cdots,k$, where: p_i and $\Delta t(i-1)$ – the magnitude and time of the ith date point of the pulse waveshape $p_j(t)$, P_i and $\Delta f(i-1)$ – the magnitude and frequency component of the ith date point of $P_j(f)$ ($\Delta t = 1/f_s$, $\Delta f = f_s/k$ and f_s is the sampling rate).

Front-ends are specifically designed for ac PD measurement to present the detection and analysis results. One of them is shown in Fig. 8. It provides a set of push-buttons to do the pulse feature extraction and unsupervised clustering of the acquired pulse sequence.

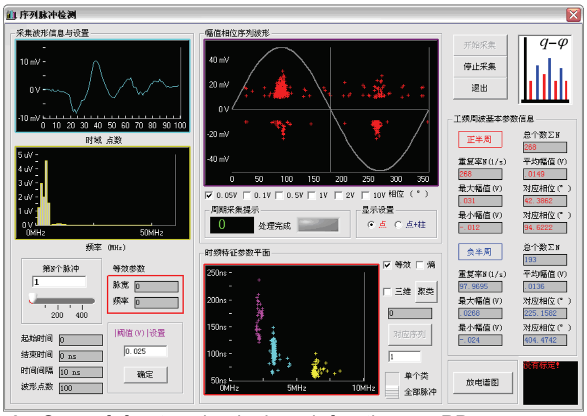

Fig.8. One of front-ends designed for the ac PD measurement system.

Experimental verification

To investigate the grouping performance of the detection system with those feature extractors for online field PD signals, the PD signals are sampled form a GIS device and two PD calibrators, respectively. The GIS device is filled with the gas SF_6 and its inside pressure strength is 0.35Mpa [21]. It is shown in Fig. 9 with the four typical PD sources made of protrusion on bus bar**,** protrusion on earth potential, floating electrode and contaminations on spacer. The simulation test of two PD calibrators was carried out in our high voltage laboratory without electromagnetic shielding.

Fig. 12, relevant to simulation PD pulse signals of two PD calibrators, one is with pulse repetition of 100Hz and waveshape shown in Fig. 12a, and another is with pulse repetition of 4Hz and waveshape shown in Fig. 12d. Unknown external noise also exists during the data sampling. Fig. 10a provides the original PD pattern of the sampled data for 400 power cycles, where both PD phenomena including pulse height and phase distributions are overlapped. The corresponding 2D and 3D feature distributions, with the optimum data partition which consists of four sub-groups, are show in Fig. 11, which give the same separation results. The typical pulse waveshapes relevant to the A, B, C and D sub-groups are reported in Fig. 12. Four different PD pattern plots can be obtained, eventually, associating each point in the A, B, C and D sub-groups are shown in Fig. 10b to 10e.

Fig. 10b to 10e show four PD patterns obtained for each sub-group, which is relevant to each PD phenomenon and external noise. Fig. 10b and 10e can be verified by their repetition rates and corresponding pulse waveshapes, which are generated by the two PD Calibrators. But for no characteristics for B and C sub-groups with their PD patterns (Fig. 10c and 10d) and corresponding pulse waveshapes, they can be judged as unknown external noise signals.

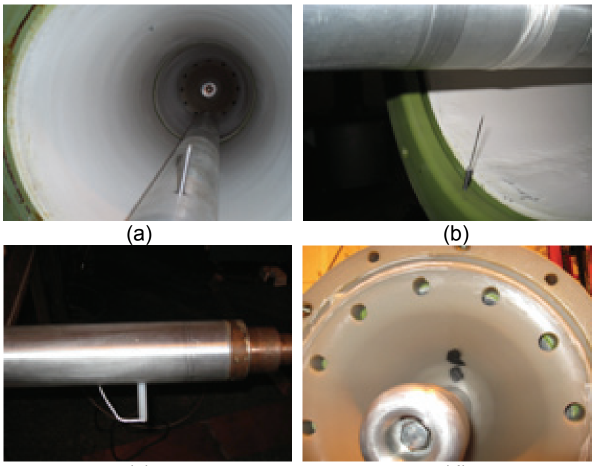

Fig.9. The inner simulation defects of GIS device (220 kV): (a) is protrusion on bus bar; (b) is protrusion on earth potential; (c) is PD defect of floating electrode; (d) is contaminations on spacer

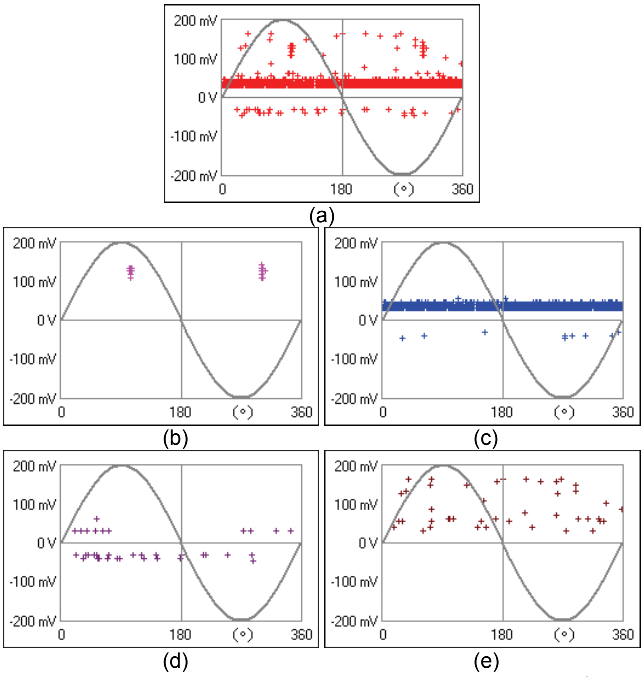

Fig.10. PD patterns: (a) is the original one; (b) is PD pattern of sub-group A; (c) is PD pattern of sub-group B; (d) is PD pattern of sub-group C; (e) is PD pattern of sub-group D

PD measurements were performed adopting the MEW with a high threshold value (10mV) in order to avoid the pulsating background noise. The sampled PD data is shown in Fig. 13a, which was collected at a certain test voltage for 200 power cycles. Fig. 13a provides the original PD pattern, where PD phenomena are mixed with random pulsed signals. The corresponding 2D and 3D feature distributions, with the optimum data partition which consists of three sub-groups, are show in Fig. 14. The typical PD pulse waveshapes in time and frequency domains relevant to the A, B and C sub-groups are reported in Fig. 15. Three different PD pattern plots can be obtained, eventually, associating each point in the A, B and C sub-groups are shown in Fig. 13b, 13c and 13d.

Fig. 13c and its waveshapes shown in Fig. 15b can be verified by its pulse height and phase distribution, which belongs to a PD phenomenon of corona discharge. So it can be judged as a PD source of the protrusion on bus bar (see Fig. 9a).

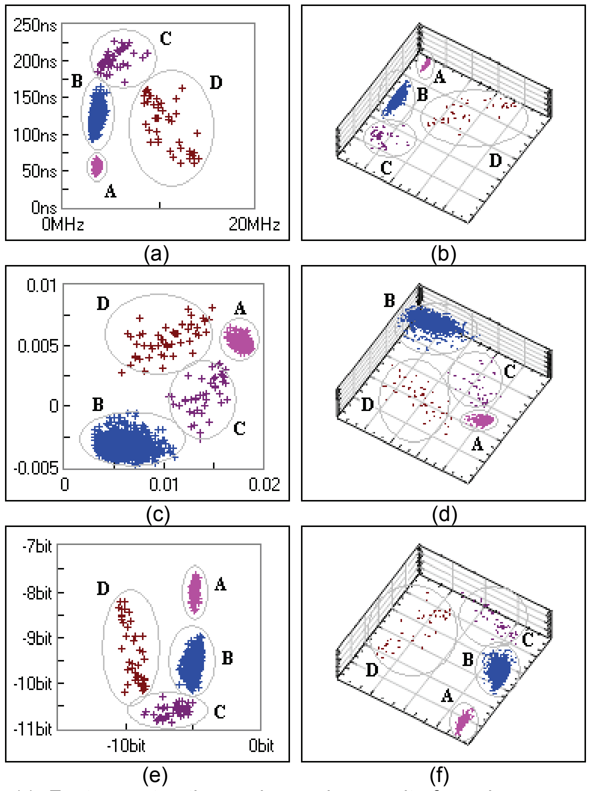

Fig.11. Feature extraction and grouping results for pulse sequence corresponding to Fig. 10a: (a) and (b) are 2D and 3D feature distributions with ETFM; (c) and (d) are 2D and 3D feature distributions with TFACM; (e) and (f) are 2D and 3D feature distributions with TFEM

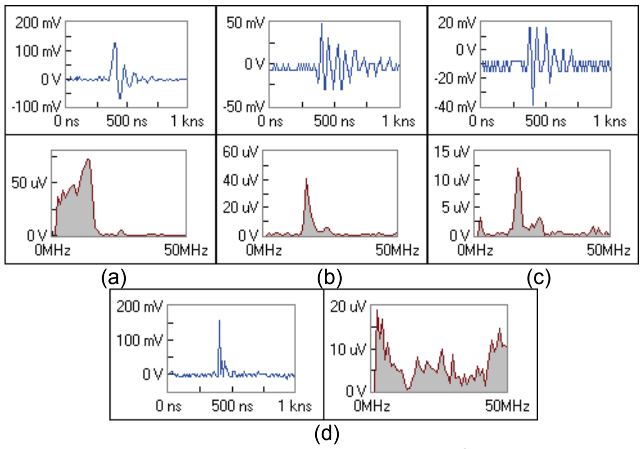

Fig.12. Typical pulse waveshapes in time and frequency domains of each sub-group in Fig. 11: (a) is from subgroup A; (b) is from subgroup B; (c) is from subgroup C; (d) is from subgroup D

The typical pulse waveshape shown in Fig. 15a and its corresponding PD pattern in Fig. 13b both indicate that it is generated by a pulsed interference signals source, and it needs the length *k* of MEW set to be a larger number to record its whole pulse waveshape in time domain. While the typical pulse waveshapes shown in Fig. 15c also have the same characteristic as a PD pulse, but its corresponding PD pattern (Fig. 13d) shows that the pulse sequence has a stochastic phase distribution which indicates it must be a random pulsed interference signal source.

PD tests were performed adopting the MEW with a high threshold value (10mV) in order to avoid the pulsating background noise. The length of MEW *k* was set to be 200 points. An interesting sampled PD data is shown in Fig. 16a for an unknown corona discharge source also active, which was collected at a certain high test voltage for 200 power cycles. Fig. 16a provides the original PD pattern. The corresponding 2D and 3D feature distributions, with the optimum data partition which consists of two sub-groups, are show in Fig. 17. The typical PD pulse waveshapes in time and frequency domains relevant to the A and B sub-groups are reported in Fig. 18. Two different PD pattern plots can be obtained, associating each point in the A and B sub-groups are shown in Fig. 16b and 16c.

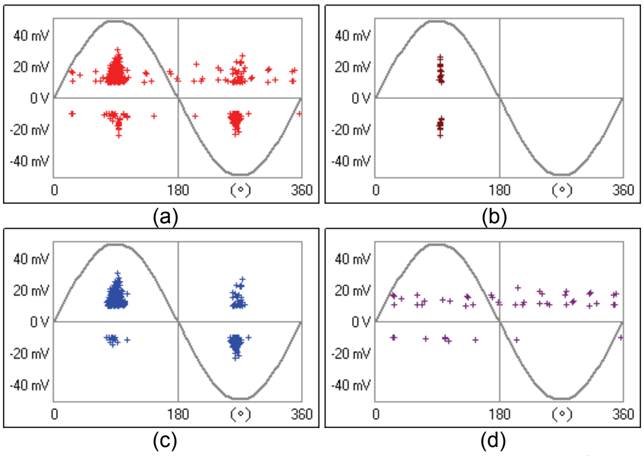

Fig.13. PD patterns: (a) is the original one; (b) is PD pattern of sub-group A; (c) is PD pattern of sub-group B; (d) is PD pattern of sub-group C.

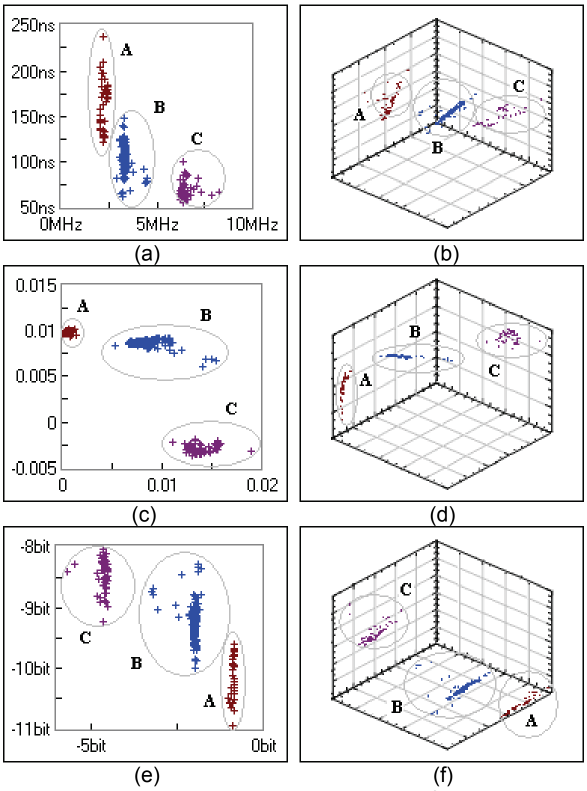

Fig.14. Feature extraction and grouping results for pulse sequence corresponding to Fig. 13a: (a) and (b) are 2D and 3D feature distributions with ETFM; (c) and (d) are 2D and 3D feature distributions with TFACM; (e) and (f) are 2D and 3D feature distributions with TFEM

Fig. 16b and its waveshapes shown in Fig. 18a can be verified by its pulse height and phase distribution, which belongs to a PD phenomenon generated by the protrusion on earth potential (see Fig. 9b). Fig. 16c and its waveshapes shown in Fig. 18b are from a PD phenomenon generated by the protrusion on bus bar, but it is an unexpected result.

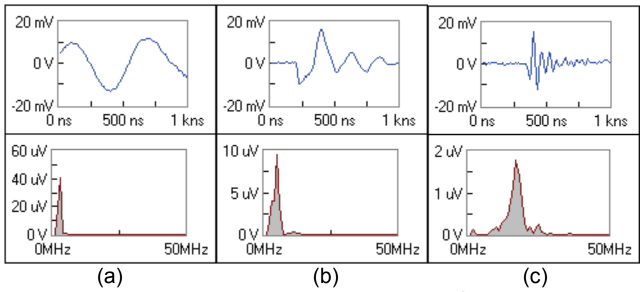

Fig.15. Typical pulse waveshapes in time and frequency domains of each sub-group in Fig. 14: (a) is from subgroup A; (b) is from subgroup B; (c) is from subgroup C

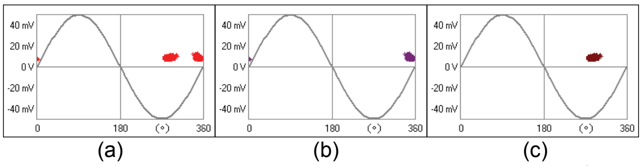

Fig.16. PD patterns: (a) is the original one; (b) is PD pattern of sub-group A; (c) is PD pattern of sub-group B

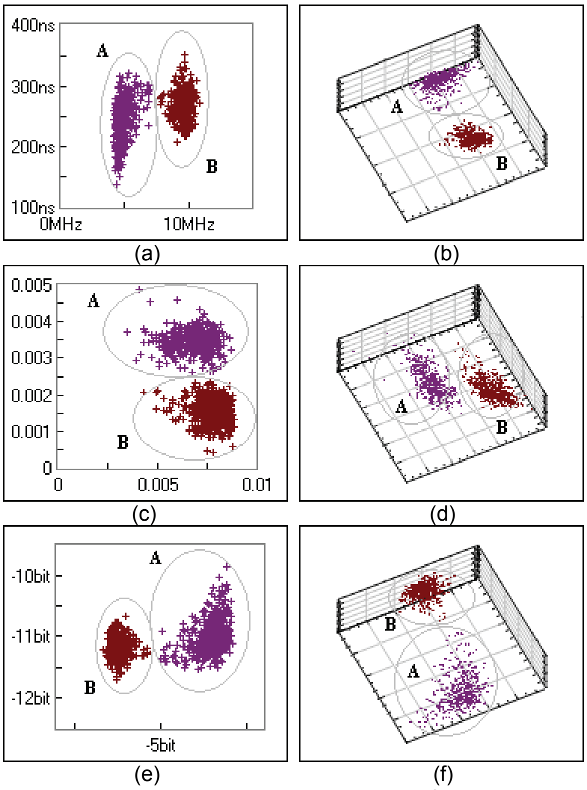

Fig.17. Feature extraction and grouping results for pulse sequence corresponding to Fig. 16a: (a) and (b) are 2D and 3D feature distributions with ETFM; (c) and (d) are 2D and 3D feature distributions with TFACM; (e) and (f) are 2D and 3D feature distributions with TFEM

For this kind of discharge can generate PD pulse signals with high amplitude, PD tests were performed adopting the MEW with a high threshold value (100mV). An example of sampled PD data is shown in Fig. 19a, which was collected at a certain test voltage for 200 power cycles. Fig. 19a provides the original PD pattern, where there are no random pulsed interference signals and it can be easily judged as a PD phenomenon of floating discharge. But the corresponding 2D and 3D feature distributions, with the optimum data partition which consists of two sub-groups, are shown in Fig. 20. The typical pulse waveshapes in time and frequency domains relevant to the A and B sub-groups are reported in Fig. 21. Two similar PD pattern plots are obtained, eventually, associating each point in the A and B sub-groups are shown in Fig. 19b and 19c.

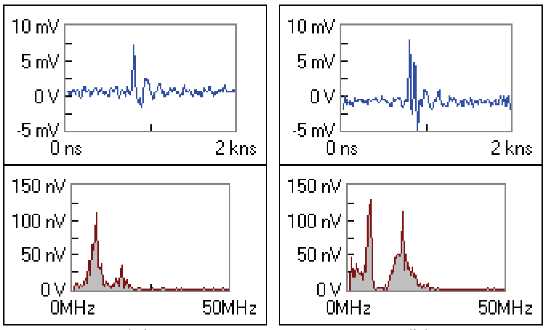

(a) (b)

Fig.18. Typical pulse waveshapes in time and frequency domains of each sub-group in Fig. 17: (a) is from subgroup A; (b) is from subgroup B

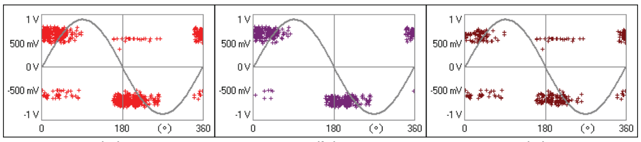

(a) (b) (c)

Fig.19. PD patterns: (a) is the original one; (b) is the PD pattern of sub-group A; (c) is the PD pattern of sub-group B

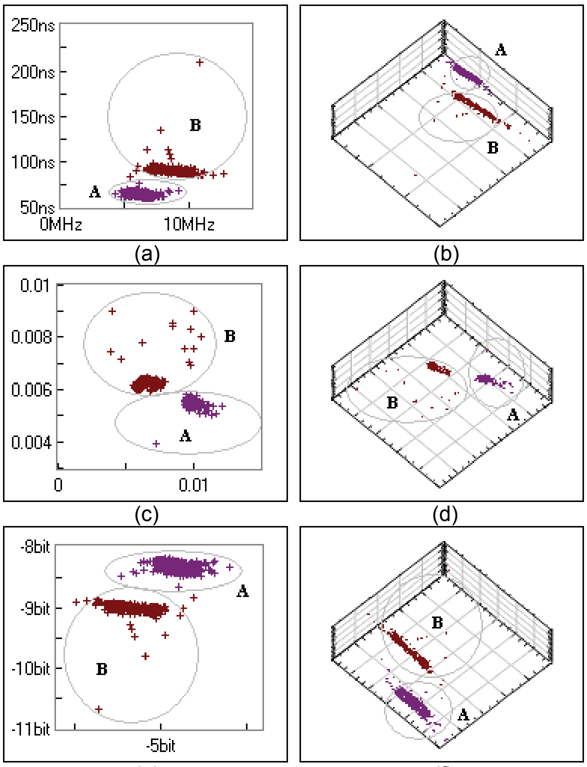

Fig.20. Feature extraction and grouping results for pulse sequence corresponding to Fig. 19a: (a) and (b) are 2D and 3D feature distributions with ETFM; (c) and (d) are 2D and 3D feature distributions with TFACM; (e) and (fd) are 2D and 3D feature distributions with TFEM

The PD pulse sequence grouping gives an unexpected result for this artificial PD defect (see Fig. 9c), because the test designer only wants one PD phenomenon of floating discharge. But both sub-groups A and B in Fig. 19 can be verified by its pulse height and phase distribution, which belongs to a PD phenomenon of floating discharge.

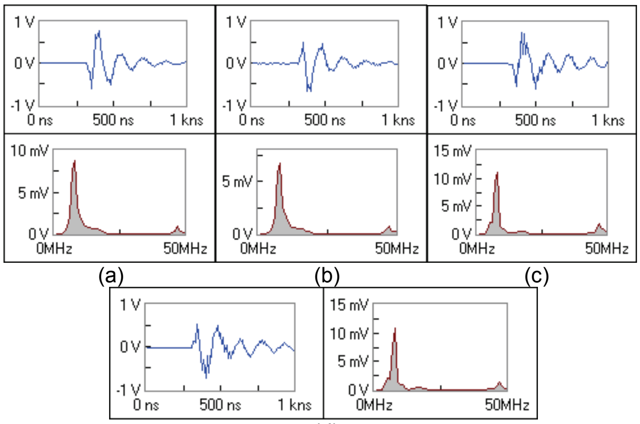

(d)

Fig.21. Typical pulse waveshapes in time and frequency domains of each sub-group in Fig. 20: (a) is from subgroup A with negative polarity; (b) is from subgroup A with positive polarity; (c) is from subgroup B with negative polarity; (d) is from subgroup B with positive polarity

Fig.22. Partial enlarged picture of floating electrode in Fig. 9c

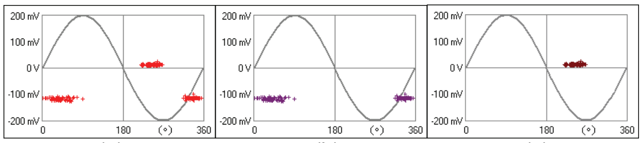

(a) (b) (c)

Fig.23. PD patterns: (a) is the original one; (b) is PD pattern of sub-group A; (c) is PD pattern of sub-group B

The typical pulse waveshapes in time domain and frequency domain of sub-group A and B shown in Fig. 21 are so similar that they can not be distinguished by purely man-made. But the feature extractors (ETFM, TFACM and TFEM) are sensitive to the tiny difference between the pulse waveshapes in time and frequency domains of sub-group A and B. For this pulse grouping results of Fig. 20 and the partial enlarged picture of floating electrode shown in Fig. 22, it may be explained that discharges happened between the floating electrode and the bus bar were not stable, and two points on the floating electrode surface could be the PD sources.

Fig. 9d shows that the PD sources are made of two contaminations on spacer. It is apparently that two kinds of PD pulses will be generated for the arrangement of contaminations. One PD source is between two contaminations and another is between the bus bar of GIS and its near contamination.

PD measurements were also performed adopting the MEW with a high threshold value (10mV) and length of 200 points. One sampled PD data is shown in Fig. 23a, which was collected at a certain test voltage for 200 power cycles.

Fig. 23a provides the original PD pattern, where PD phenomena are not overlapped. The corresponding feature extraction results shown in Fig. 24 consist of two sub-groups. Two typical PD pulse waveshapes relevant to the A and B sub-groups are reported in Fig. 25. And two PD patterns plots are also obtained, associating each point in the A and B sub-groups shown in Fig. 23b and 23c.

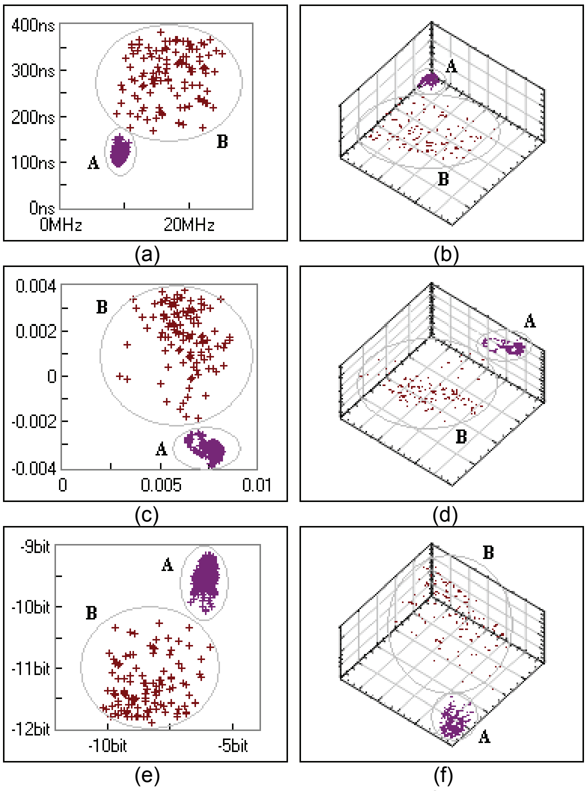

Fig.24. Feature extraction and grouping results for pulse sequence corresponding to Fig. 23a: (a) and (b) are 2D and 3D feature distributions with ETFM; (c) and (d) are 2D and 3D feature distributions with TFACM; (e) and (f) are 2D and 3D feature distributions with TFEM

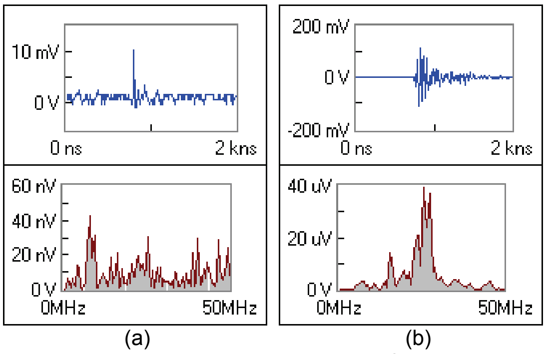

Fig.25. Typical pulse waveshapes in time and frequency domains of each sub-group in Fig. 24: (a) is from subgroup A; (b) is from subgroup B

Discussion

The above results show that this digital ac PD measurement system is capable of handling noise rejection for PD sources resorting to the recorded pulse waveshapes. Features related to pulse waveshapes introduced in section 2 (ETFM, TFACM and TFEM), can provide a significant contribution to solve the grouping problem when different kinds of pulse sources provide different signal waveshapes. Good results are obtained when the pulse height and phase distributions are overlapped, even the difference between the pulse waveshapes in time and frequency domains are tiny.

The FFT is chosen as the transform to make feature extraction for PD pulse waveshape with consideration of a good compromise between complexity of computations and real-time requirements. This powerful tool lies at the base of the concepts of frequency spectrum and frequency response. As we all know, the FT is perfectly applicable to infinite and periodic signals since it is based on the assumption that any signal can be decomposed into a series of sine or cosine waveforms. Other popular and effective transforms, such as fast Mellin transform (FMT) [22], independent component analysis (ICA) [19], and Hilbert-Huang transform (HHT) [23], etc, can also be put into consideration for the PD pulse feature extraction, if the formed feature parameters are with good separability to stochastic pulse waveshapes of different PD sources or pulsed interference signals.

In this paper, how to make and evaluate the feature extraction methods of PD pulse waveshape used in sequence grouping are discussed, all of which meet the needs of online monitoring of PD data in real-time. For post processing of PD data not in real-time, some feature extractor such as principal component analysis (PCA), singular value decomposition (SVD), and Wigner-Ville distribution (WVD) [18], etc, can also be chosen as feature extractors of PD pulse waveshape, although they are time and memory consuming.

Conclusions

A general way to make feature extraction for PD pulse waveshape used in sequence grouping is presented. Three feature extractors are obtained with different post-processing to pulses in time and frequency domains, which are equivalent evaluation, autocorrelation and information measure. A separability criterion for PD pulse feature extractors is defined and how to generate PD pulse sequence with Monte Carlo simulation based on exponential models is presented, which is used to evaluate the grouping performance of those feature extractors in theoretically. The analysis results show that all feature extractors have good performance used in PD pulse sequence grouping. To investigate the grouping performance of the detection system with those feature extractors for an online field PD signals, a simple digital ac PD pulse detection system with bandwidth of 10 kHz – 40 MHz and sampling rate of 100 MS/s is introduced. Experimental verification is made resorting to the ac PD detection system with GIS artificial defect models and two PD calibrators respectively, which shows that those feature extractors are practical and effective to develop the PD pulse measurement system with grouping technique to deal with noise rejection and multi-PD sources.

REFERENCES

[1] Gulski E., Chojnowski P., Rakowska A., Importance of sensitive on-site testing and diagnosis of transmission power cables, *Przegląd Elektrotechniczny*, 85 (2009), No. 2, 171-176

[2] Noske S., Rakowska A., Siodla K., Measurements of partial discharges as source of management knowledge improvement of the power calbe network, *Przegląd Elektrotechniczny*, 84 (2008), No. 10, 12-15

[3] Ziomek W., Kuffelz E., Sikorski W., Location and recognition of partial discharge sources in power transformer using advanced acoustic emission method, *Przegląd Elektrotechniczny*, 84 (2008), No. 10, 20-23

[4] Szadkowski M., Image of a partial discharge between two conductors which are rapidly changing position against themselves, *Przegląd Elektrotechniczny*, 84 (2008), No. 10, 203-206

[5] Gulski E.,Piepers OM.,Majsymiuk J., Analysis of condition data of high voltage components, *Przegląd Elektrotechniczny*, 83 (2007), No. 12, 64-68
[6] IEC 60270, Partial discharge Measurements, 3rd ed., Mar. 2001
[7] Judd M.D, Farish O., Pearson S.J, Dielectric windows for UHF partial discharge detection, *IEEE Transactions on Dielectrics and Electrical Insulation*, 8 (2001), No. 1, 953-958
[8] Lundqaard L.E., Partial discharge. XIV. Acoustic partial discharge detection - practical application, *IEEE Electrical Insulation Magazine*, 8 (1992), No. 3, 34-43
[9] Wang X.D., Li, Z B.Q., Roman H., An ultra-sensitive optical MEMS sensor for partial discharge detection, *Journal of Micromechanics Microengineering*, 15 (2005), No. 8, 521-527
[10] Contin A., Cavallini A., Montanari G.C., Pasini G., Digital detection and fuzzy classification of partial discharge signals, *IEEE Transactions on Dielectrics and Electrical Insulation*, 9 (2002), No. 12, 335-348
[11] Cavallini A., Contin A., Montanari G.C., Puletti F., Advanced PD inference in on-field measurements, part 1: noise rejection, *IEEE Transactions on Dielectrics and Electrical Insulation*, 10 (2003), No. 3, 528-537
[12] Cavallini A., Montanari G.C., Puletti F., Contin A., A new methodology for the identification of PD in electrical apparatus: properties and applications, *IEEE Transactions on Dielectrics and Electrical Insulation*, 12 (2005), No.12, 203-214
[13] Si Wenrong, Li Junhao, Li Yanming, Digital detection, grouping and classification of partial discharge signals at DC voltage, *IEEE Transactions on Dielectrics and Electrical Insulation*, 15 (2008), No. 6, 1663-1664
[14] Babnik T., Aggarwal R.K., Moore P.J., Principal component and hierarchical cluster analyses as applied to transformer partial discharge data with particular reference to transformer condition monitoring, *IEEE Transactions on Power Delivery*, 1 (2008), No. 2, 1-9
[15] Yan W.Z., Goebel K.F., Feature selection for partial discharge diagnosis, *Proceedings of the 12th SPIE*: Health Monitoring and Smart Nondestructive Evaluation of Structural and Biological System IV, 5768 (2005), 166-175
[16] Si Wenrong, Li Junhao, Li Yanming, The fast grouping technique of PD sequence based on the nonlinear mapping of pulse shapes, *Transactions Of China Electrotechnical Society*, 23 (2009), No. 3, 216-221
[17] Si Wenrong, Li Junhao, Li Yanming, Fast feature extraction technique for PD pulse shape based on wideband detection, *Advanced Technology of Electrical Engineering and Energy*, 27 (2008), No. 2, 21-25
[18] Si Wenrong, Li Junhao, Li Yanming, Time-frequency analysis on pulse current of parital dishcharge, *Przegląd Elektrotechniczny*, 85 (2009), No. 7, 40-44
[19] Si Wenrong, Li Junhao, Li Yanming, Stuyd on white noise suppression for PD signals using ICA, *Przegląd Elektrotechniczny*, 85 (2009), No. 12, 252-257
[20] Hikita M., Yamada K., Nakamura A., Mizutani T., Oohasi A., Measurements of partial discharges by computer and analysis of partial discharge distribution by the Monte Carlo method, *IEEE Transactions on Electrical Insulation*, 25 (1990), No. 12, 453-468
[21] Si Wenrong, Li Junhao, Yuan Peng, Li Yanming, Detection and identification techniques for multi-PD source in GIS, *Proceedings of the CSEE*, 29 (2009), No.16, 119-126
[22] Si Wenrong, Li Junhao, Guo Hong, Li Yanming, A new method for frequency-domian transform of PD pulse, *High Voltage Apparatues*, 44 (2008), No. 5, 453-455
[23] Wang X.D., Li B.Q., Liu Z.W., Roman H.T., Farmer K.R., Analysis of partial discharge signal using the Hilbert-Huang transform, *IEEE Transactions on Power Delivery*, 21 (2006), No. 12, 1063-1067

***Authors**: Dr. Si Wenrong, East China Electric Power Test & Research Institude Company Limited, Shanghai, China, 200437, E-mail: siwenrong@gmail.com; Dr. Fu Chenzhao, East China Electric Power Test & Research Institude Company Limited, Shanghai, China, 200437, E-mail: dsy_fucz@ec.sgcc.com.cn；Dr. Gao Kai, East China Electric Power Test & Research Institude Company Limited, Shanghai, China, 200437, E-mail: dsy_gaok@ec.sgcc.com.cn.*